Original Article

MOLECULAR METABOLISM

Neuroanatomical organization and functional roles of PVN MC4R pathways in physiological and behavioral regulations

Uday Singh [1], Jingwei Jiang [1], Kenji Saito [1], Brandon A. Toth [1], Jacob E. Dickey [1], Samuel R. Rodeghiero [1], Yue Deng [1], Guorui Deng [1], Baojian Xue [2], Zhiyong Zhu [3], Leonid V. Zingman [3], Joel C. Geerling [4,6], Huxing Cui [1,5,6,7,*]

ABSTRACT

Objective: The paraventricular nucleus of hypothalamus (PVN), an integrative center in the brain, orchestrates a wide range of physiological and behavioral responses. While the PVN melanocortin 4 receptor (MC4R) signaling (PVN^{MC4R+}) is involved in feeding regulation, the neuroanatomical organization of PVN^{MC4R+} connectivity and its role in other physiological regulations are incompletely understood. Here we aimed to better characterize the input—output organization of PVN^{MC4R+} neurons and test their physiological functions beyond feeding.

Methods: Using a combination of viral tools, we mapped PVN^{MC4R+} circuits and tested the effects of chemogenetic activation of PVN^{MC4R+} neurons on thermoregulation, cardiovascular control, and other behavioral responses beyond feeding.

Results: We found that PVN^{MC4R+} neurons innervate many different brain regions that are known to be important not only for feeding but also for neuroendocrine and autonomic control of thermoregulation and cardiovascular function, including but not limited to the preoptic area, median eminence, parabrachial nucleus, pre-locus coeruleus, nucleus of solitary tract, ventrolateral medulla, and thoracic spinal cord. Contrary to these broad efferent projections, PVN^{MC4R+} neurons receive monosynaptic inputs mainly from other hypothalamic nuclei (preoptic area, arcuate and dorsomedial hypothalamic nuclei, supraoptic nucleus, and premammillary nucleus), the circumventricular organs (subfornical organ and vascular organ of lamina terminalis), the bed nucleus of stria terminalis, and the parabrachial nucleus. Consistent with their broad efferent projections, chemogenetic activation of PVN^{MC4R+} neurons not only suppressed feeding but also led to an apparent increase in heart rate, blood pressure, and brown adipose tissue temperature. These physiological changes accompanied acute transient hyperactivity followed by hypoactivity and resting-like behavior.

Conclusions: Our results elucidate the neuroanatomical organization of PVN^{MC4R+} circuits and shed new light on the roles of PVN^{MC4R+} pathways in autonomic control of thermoregulation, cardiovascular function, and biphasic behavioral activation.

Keywords Melanocortin 4 receptor; Paraventricular nucleus of hypothalamus; Blood pressure; Thermoregulation; Sympathetic nervous activity

1. INTRODUCTION

Obesity is a major risk factor for the development of hypertension; several population studies indicate that at least two thirds of the prevalence of hypertension can be directly attributed to obesity [1]. Sympathetic overactivity has been established in obese individuals and is considered one of the major contributors to the development of obesity-associated hypertension [2,3]. Mounting evidence indicates that the central melanocortin signaling pathway, mainly via melanocortin 4 receptor (MC4R), plays a key role in obesity [4—7]. Besides having a prominent role in energy homeostasis [8,9], MC4R signaling pathways are known to affect the sympathetic activity and cardiovascular physiology. Central administration of MC4R agonist steadily increases blood pressure (BP) and sympathetic traffic to various organs, including the kidney [10—12]. In contrast to the elevated sympathetic tone and BP commonly observed in obesity, morbidly obese humans and rodents due to monogenic MC4R-deficiency exhibit low to normal sympathetic nerve activity (SNA) and BP [13—17], suggesting a required but dissociable role of MC4R signaling in both metabolic and cardiovascular regulations in the context of obesity. Notably, accumulating evidence indicates the need for MC4R for leptin-induced sympathoexcitation; both pharmacological and genetic blockade of

[1]Department of Neuroscience and Pharmacology, University of Iowa Carver College of Medicine, Iowa City, IA, United States [2]Department of Psychological and Brain Sciences, University of Iowa, Iowa City, IA, United States [3]Department of Internal Medicine, University of Iowa Carver College of Medicine, Iowa City, IA, United States [4]Department of Neurology, University of Iowa Carver College of Medicine, Iowa City, IA, United States [5]F.O.E. Diabetes Research Center, University of Iowa Carver College of Medicine, Iowa City, IA, United States [6]Iowa Neuroscience Institute, University of Iowa Carver College of Medicine, Iowa City, IA, United States [7]Obesity Research and Educational Initiative, University of Iowa Carver College of Medicine, Iowa City, IA, United States

*Corresponding author. Department of Neuroscience and Pharmacology, University of Iowa Carver College of Medicine, 51 Newton Road, 2-372 Bowen Science Building, Iowa City, IA, 52242, United States. Fax: +319 335 8930. E-mail: huxing-cui@uiowa.edu (H. Cui).

Received October 5, 2021 • Revision received November 4, 2021 • Accepted November 17, 2021 • Available online 22 November 2021

https://doi.org/10.1016/j.molmet.2021.101401

MC4R abolish the leptin-mediated increase in sympathetic traffic to the kidney [11,12,18]. Moreover, central infusion of MC4R antagonist significantly decreases BP even in spontaneously hypertensive rats with normal body weight [17], thereby confirming the vital role of the MC4R signaling pathway in neurogenic hypertension beyond obesity. While the above studies underscore physiologically important roles for brain MC4R signaling in sympathetic activity and BP regulation, the neural basis underlying MC4R regulation of sympathetic control of cardiovascular function remains poorly understood.

The paraventricular nucleus of hypothalamus (PVN), an indispensable integrative center in the brain, coordinates numerous physiological and behavioral responses, such as feeding, metabolic homeostasis, and sympathetic control of cardiovascular function, via its connections to diverse brain regions including different brainstem nuclei and spinal cord [19]. Importantly, the PVN has the highest expression of MC4R among other hypothalamic and brainstem nuclei [20,21]; PVN^{MC4R} signaling has been well known for its role in the regulation of feeding and body weight homeostasis [22–24]. Additionally, a pharmacological study has shown that PVN^{MC4R} signaling may also affect the sympathetic activity and BP regulation. Microinjection of MC4R agonist directly into the PVN of anesthetized mice increases BP and sympathetic traffic to the kidney through canonical MC4R-Gαs-cAMP-PKA pathway [25]. This finding was supported by another study that showed that the ability of systemic MC4R agonist to increase BP is lost in mice lacking Gαs in entire PVN neurons [26]. Remarkably, a slice electrophysiological study has shown that MC4R agonist increases the firing of the rostral ventrolateral medulla (RVLM)-projecting presympathetic PVN neurons in Zucker rats [27], with a greater increase of firing activity in obese rats compared to lean controls. This suggests that enhanced activity of PVN^{MC4R} signaling pathway may underlie obesity-associated hypertension. While these pharmacological and *ex vivo* electrophysiological approaches support a role for PVN^{MC4R} signaling in sympathetic control of cardiovascular function, the neuroanatomical organization of PVN^{MC4R} pathways and the effects of selective activation of PVN^{MC4R+} neurons on cardiovascular and other behavioral and physiological parameters remains unclear.

In the present study, we mapped PVN^{MC4R} circuits using a combination of viral tools and tested the hypothesis that indiscriminate activation of PVN^{MC4R+} neurons not only affects feeding but also other behavioral physiological parameters through their diffuse projections to brain regions associated with autonomic and behavioral responses.

2. METHODS

2.1. Animals

MC4R-2a-Cre knock-in mice (Jackson Stock No: 030759) were obtained from Dr. Brad Lowell group [24]. Mice were group-housed in the University of Iowa's vivarium in a temperature-controlled environment (lights on 06:00, Light off 18:00) with free access to standard chow diet and water. Mice used in the present study were all maintained in C57BL/6 and 129 mixed backgrounds. All animal protocols were approved by the Institutional Animal Care and Use Committee of the University of Iowa; and are as per NIH guidelines for the use and care of Laboratory Animals.

2.2. Viral vectors for neuronal tracing

Viral vectors from different scientific vendors were used to examine the neuroanatomical organization and the functional roles of PVN^{MC4R+} circuits, including Cre-dependent AAV2-DIO-ChR2-eYFP (Addgene), AAV2-DIO-mCherry (Addgene), AAV2-DIO-hM3Dq-mCherry (Addgene), AAV-retro-DIO-Flp (Duke Viral Vector Core); Flp-dependent AAV8-fDIO-TVA-mCherry (Salk Institute Viral Vector Core) and AAV8-fDIO-G (Salk Institute Viral Vector Core); and glycoprotein-deleted rabies virus (RV-EnvA-ΔG-GFP, Salk Institute Viral Vector Core).

2.3. Stereotaxic surgery

Stereotactic surgery was performed as previously described [28]. Briefly, male MC4R-Cre+ mice were deeply anesthetized by intraperitoneal (IP) injection of ketamine/xylazine (100:10 mg/kg) and placed on a Kopf stereotaxic apparatus (Tujunga, CA). Following standard disinfection procedure, ~1.0 cm incision was made to expose the skull of the mice and a small hole was drilled into the skull bilaterally at defined positions to target the PVN (coordinates: AP -0.8 mm, ML +1.1 mm, DV -4.9 mm with 10-degree injection arm). Pulled glass micropipette filled with a viral vector was slowly inserted to reach the targeted brain region and a small volume (150–200 nl) of injection was made by applying pulse pressure using Tritech pressure Microinjector (Tritech Research, Los Angeles, CA). After 10 min of waiting to ensure full penetration of the injectant into the targeted area, the needle was slowly removed and the incision closed by wound clips. Then, the mice were kept on a warming pad until awake and fed a regular chow diet throughout the experimental period unless otherwise required.

2.4. Fluorescent double immunohistochemistry (IHC)

Brains of all mice that received viral injection were processed for histological verification of correct stereotaxic targeting. Immunohistochemistry (IHC) was performed as previously reported [28,29]. Briefly, the mice were transcardially perfused with cold Phosphate-buffered saline (PBS) followed by 10% neutralized formalin; the brains were removed and immersed in 25% sucrose solution; brains were cut into five series of 30 μm sections, and then stored in cryoprotectant at −20 °C until processed for IHC. One series of brain sections were rinsed in PBS, blocked in 3% normal donkey serum and 0.3% Triton X-100 in PBS for 30 min at room temperature. The sections were then incubated with primary antibodies against GFP (Cat# GFP-1020, Aves Labs), mCherry (Cat# 632496, Clontech), or c-Fos (Cat# PC38, Cal-BioChem) overnight at 4 °C, and then washed and incubated with Cy2- or Cy3-conjugated secondary antibodies (Jackson ImmunoResearch) for fluorescent visualization, as per the manufacturer's protocols.

2.5. Neuroanatomical tracing of input–output organization of PVN^{MC4R+} neurons

For the mapping of efferent projections PVN^{MC4R+} neurons, adult MC4R-Cre+ male mice (12–20 weeks old) received a unilateral stereotaxic injection of AAV2-DIO-ChR2-eYFP (~150 nl) into the PVN using a glass micropipette pressure injection system, as described above. After 3–4 weeks of viral injection, the mice were transcardially perfused with 10% neutralized formalin, and the whole brains were cut into five series of 30 μm sections and then stored in cryoprotectant at −20 °C until further processed for IHC. Brain sections were processed for fluorescent IHC for eYFP (using chicken anti-GFP antibody, Cat# GFP-1020, Aves Labs) and the sections were mounted onto gelatin-coated slides for microscopic imaging. The slides were imaged using a slide-scanning microscope (VS120, Olympus) and the images were captured and analyzed using the OlyVIA software. Only correctly targeted four cases with minimal contamination to adjacent brain regions were used for whole-brain manual qualitative evaluation of efferent projections.

For whole-brain mapping of monosynaptic inputs to PVN^{MC4R+} neurons, a mixture of AAV-DIO-flp (Cre-dependent) and Flp-dependent AAV8-fDIO-TVA-mCherry and AAV8-fDIO-RV-G was unilaterally injected into

the PVN of MC4R-Cre+ mice using glass micropipette pressure injection system, as aforementioned. After three weeks of stereotaxic surgery, a small volume (~100 nl) of glycoprotein-deleted rabies virus (RV-EnvA-ΔG-GFP) was injected into the same side of PVN where a mixture of AAV was previously infused. One week post-RV-EnvA-ΔG-GFP injection, the mice were transcardially perfused with 10% neutralized formalin, and the whole brains were cut into five series of 30-μm sections and then stored in cryoprotectant at −20 °C until further processed for IHC. One series of brain sections from each brain were processed for fluorescent IHC for GFP and the sections were then mounted onto coated microscope slides for imaging. Slides were imaged by a slide-scanning microscope (VS120, Olympus) and the images were captured and analyzed using OlyVIA software. Only correctly targeted cases with minimal contamination to adjacent brain regions (n = 4) were used for the brain-wide manual qualitative evaluation of neurons sending monosynaptic inputs to PVN^{MC4R+} neurons.

2.6. Feeding and glucose homeostasis

The effect of designer receptor exclusively activated by designer drugs (DREADD) activation of PVN^{MC4R+} neurons on feeding and glucose homeostasis was evaluated in two independent cohorts of experimental mice. Cohort 1 had adult (10−16 weeks) MC4R-Cre+ male mice (n = 7) that received a stereotaxic injection of AAV2-DIO-hM3Dq-mCherry into the PVN. For feeding, *ad lib*-fed mice were divided into two groups and they received intraperitoneal (IP) injection of either saline or small molecule DREADD receptor agonist clozapine-N-oxide (CNO; 2 mg/kg) right before the onset of dark cycle (6 PM) and food intake was measured manually at 2- and 4-hour post-injection. CNO was administered at a volume (μL) of 10X body weight in grams. The same experiment was repeated the next day but with crossover treatment. For glucose homeostasis, 2−3 h fasted mice were divided into two groups and measured for baseline glucose using a small volume of blood drawn from the tail followed by IP injection of either saline or CNO (2 mg/kg). Blood glucose was again measured at 30-, 60-, and 120-min post-injection. The same measurement was performed the next day but with a crossover treatment. After one week of resting, the mice fasted for five hours underwent a glucose tolerance test (GTT; 1 g/kg) with 15-min pretreatment of either saline or CNO (2 mg/kg). After one week of resting, GTT was performed again but with crossover treatment. Cohort-2 consists of adult (10−16 weeks) MC4R-Cre+ male mice that received stereotaxic injection of either AAV2-DIO-hM3Dq-mCherry (DREADD group, n = 8) or AAV2-DIO-mCherry (control group, n = 7) into the PVN. For feeding, mice were singly housed in customized home cage attached with Feeding Experimentation Device 3 (FED3, Open Ephys) through a customized window on the side of cage such that mouse can obtain 20 mg food pellet (F0163, Bio-Serv) from FED3 pellet tray accessible inside of home cage by making correct nose poke [30]. Mice were fully trained to consume food pellets in this customized, FED3-attached home cage under fixed ration 1 (FR1) schedule (one correct nose poke to deliver one 20 mg food pellet) before functional evaluation of PVN^{MC4R+} neuron activation on feeding. On the test day, the mice were given IP injection of CNO (2 mg/kg) right before dark phase and the consumption of pellets was continuously monitored for additional 24 h. For the effect of PVN^{MC4R+} neuron activation on GTT, mice were fasted for five hours and they received IP injection of CNO (2 mg/kg) 15 min before IP injection of glucose (1 g/kg) and blood glucose was measured at 0-, 15-, 30-, 60-, and 120-min time points, and their levels were compared between the groups.

2.7. Body surface temperature

Cohort-1 experimental mice from the feeding study (n = 7) were subjected to infrared (IR) temperature measurement using a high-resolution infrared camera (A655sc Thermal Imager; FLIR Systems, Inc.) as described previously [31]. Again, a crossover design was used to evaluate the effects of PVN^{MC4R+} neuron activation on thermoregulation. Briefly, the mice were imaged on a multilane treadmill (without active shock grid turned on) during 3 min of slow walking (7 m/min and 15° incline), as published previously [32]. Images were captured at 1fps. Ten images were quantified for each time point using FLIR ResearchIR software (version 3.4.13039.1003) and intensity was averaged for making group comparison. After the measurement of baseline temperature, the mice received IP injection of either saline or CNO (2 mg/kg) and were then returned to their home cages. The body surface temperature was monitored again 1-h post-injection and the change in temperature from the baseline was determined and compared between the groups.

2.8. Core body temperature

Cohort-2 experimental mice from the feeding study were subjected to the measurement of core body temperature upon DREADD activation of PVN^{MC4R+} neurons. To this end, both groups of DREADD (n = 8) and control (n = 7) mice were implanted with temperature transponders (IPTT-300 HTEC, Bio Medic Data Systems) into the abdominal cavity. After one week of recovery from the surgery, both groups of mice were given IP injection of CNO (2 mg/kg) and the core body temperature was monitored every 10 min up to 90 min in their home cages using a Temperature Probe Reader (DAS-8027IUS, Bio Medic Data Systems). The change in core body temperature from the baseline (before CNO injection) was calculated for each mouse and compared between the groups.

2.9. Behavioral measurements in PhenoTyper cages

Cohort-1 experimental mice from the feeding study (n = 7) were subjected to behavior characterization using Model 3000 Noldus PhenoTyper chambers (Noldus, Wageningen, Netherlands), as earlier described [33]. PhenoTyper chamber has an infrared CCD camera installed on the top, which allows automated tracking of mouse movement throughout the experimental period. White shredded paper bedding was given on the floor to mimic a home cage-like environment. The arena floor (30 × 30 cm) was further divided into 4 sub-arenas, namely wheel running, food, water, and shelter zones (Figure 6A). Video tracking and quantification of mouse behaviors were performed using EthoVision XT 15 software (Noldus Information Technology). Mice were acclimated in the chambers overnight prior to the testing. A crossover design was used to evaluate behavioral changes in response to chemogenetic activation of PVN^{MC4R+} neurons. The distance traveled within arena, body mobility, the time spent in food and shelter zones, the number of water licks, and wheel-running activity were quantified and compared between the groups. At the end of the experiment, mice were transcardially perfused with 10% neutralized formalin and brains were extracted for histological verification of stereotaxic targeting.

2.10. Radio-telemeter implantation and BP measurements

Adult (10−16 weeks) MC4R-Cre+ male mice that received a stereotaxic injection of either AAV2-DIO-hM3Dq-mCherry (DREADD group, n = 6) or AAV2-DIO- mCherry (control group, n = 3) into the PVN were subjected to radio-telemetry implantation (PA-C10, Data Science

Instruments) for continuous BP and heart rate (HR) monitoring, as previously reported [34]. Briefly, animals were deeply anesthetized with ketamine/xylazine (100 mg/10 mg/kg) and then kept on a heating pad to ensure proper maintenance of body temperature. Topical application of eye ointment was given to minimize corneal desiccation. Radio-telemeters were disinfected in actril solution overnight and then kept in sterile saline prior to surgical implantation. Under aseptic surgical conditions, the catheter of the radio-telemeter was inserted into the left carotid artery and tied securely using a 6-0 surgical suture. The transmitter was tunneled subcutaneously from the neck until the unit reached the midabdominal region. The neck incision was sutured closed with 4-0 absorbable cat gut and then further sealed with tissue adhesive (Vet-Bond) along the incision line. Warmed sterile saline (500 μl) was given subcutaneously and the animals were kept on a heating pad until awake.

After about two weeks of recovery from the surgery, both mouse groups were subjected to the measurements of BP and HR in their home cages. Mice were handled and subjected to mock IP injection daily (at random times) for 4–5 days to minimize the confounding effects of handling and stress induced by IP injection. On the test day, the mice were given IP injection of CNO (2 mg/kg) in the morning (~8 AM) and then again in the evening right before the dark cycle (18:00) to evaluate circadian effects of DREADD activation of PVN^{MC4R+} neurons on cardiovascular function. BP was continuously monitored and analyzed by the PhysioTel CONNECT system and LabChart software (ADInstruments). At the end of the experiment, mice were transcardially perfused with 10% neutralized formalin and brains were extracted for histological verification of correct targeting of hM3Dq-mCherry in the PVN.

2.11. Statistical analyses

Statistical analyses were performed using GraphPad Prism (GraphPad Software, La Jolla, CA) software. Comparisons were made by Student's t-test, multiple t-tests, or two-way ANOVA with Holm-Sidak post-hoc analysis as previously noted. Value of $P < 0.05$ was considered statistically significant. Data are presented as mean ± SEM.

3. RESULTS

3.1. PVN^{MC4R+} neurons broadly innervate brain regions involved in feeding, neuroendocrine regulation, and autonomic control

To understand the neuroanatomical organization of PVN^{MC4R} pathways, we performed viral-mediated anterograde tract-tracing of PVN^{MC4R+} neurons. Unilateral microinjection of Cre-dependent AAV2-DIO-ChR2-eYFP was made into the PVN of MC4R-Cre mice (Figure 1A). After 3–4 weeks, mice were transcardially perfused with 10% formalin and brains were processed for fluorescent IHC. Imaging of eYFP immunoreactivity confirmed four precisely targeted cases with minimal transduction of neurons outside the PVN (Supplemental Figure 1). Subsequent evaluation of the distribution of eYFP fibers revealed that PVN^{MC4R+} neurons (Figure 1B) broadly innervate different brain regions involved in feeding, thermoregulation, neuroendocrine function and autonomic regulation, including but not limited to the bed nucleus of the stria terminalis (BNST), preoptic area (POA), lateral hypothalamic area (LHA), the dorsomedial nucleus of hypothalamus (DMH), ventromedial nucleus of hypothalamus (VMH), arcuate nucleus of hypothalamus (ARC), median eminence (ME), anterior paraventricular thalamic nucleus (PVA), periaqueductal gray (PAG), parabrachial nucleus (PBN), pre-locus coeruleus (pre-LC), nucleus of solitary tract (NTS), the dorsal motor nucleus of the vagus (DMV), rostral and caudal ventrolateral medulla (RVLM and CVLM), and thoracic spinal cord (TSC) (Figure 1C-Y). Qualitative visual estimation of relative eYFP fiber density across brain regions is summarized in Supplemental Table 1. Notably, the projections to most brain regions were largely unilateral (Supplemental Figure 2A-N), except PVA, NTS, and DMV where we observed a strong bilateral innervation of PVN^{MC4R+} neurons (Figure 1V and Supplemental Figure 2C and N).

3.2. Mapping of monosynaptic inputs to PVN^{MC4R+} neurons

After the whole brain mapping of afferent projections of PVN^{MC4R+} neurons, we aimed to determine the brain regions where neurons send monosynaptic inputs to PVN^{MC4R+} neurons. For this purpose, we injected a combination of AAVs driving the expression of TVA and glycoprotein (G) that are required for cell-type-specific monosynaptic inputs into the PVN (Figure 2A,B). After 3 weeks, EnvA-pseudotyped G-deleted Rabies viruses (RV-EnVA-ΔG-GFP) were again injected into the PVN of the MC4R-Cre^{+} mouse to label neurons sending monosynaptic inputs to PVN^{MC4R+} neurons, as previously reported [36]. Contrary to broad efferent projections, we observed monosynaptic labeling (GFP+ neurons) in relatively limited brain regions (observations made from four successfully targeted cases), mainly other hypothalamic nuclei, including ARC, DMH, POA (MPO, MnPO, and LPO), SON, VMH, LHA, and PMN (Figure 2E–F, 2H–K). We also documented that neurons in two circumventricular organs, the subfornical organ (SFO) and organum vasculosum of the lamina terminalis (OVLT), make monosynaptic inputs to PVN^{MC4R+} neurons (Figure 2E,G). We observed a large number of GFP+ neurons in BNST and PBN (Figure 2D–F, 2N), and sparse GFP+ neurons in DRN, PAG, vSUB, and NTS (Figure 2L–M, O). Overall patterns of monosynaptic inputs to PVN^{MC4R+} neurons are summarized in the schematic shown in Figure 2P.

3.3. DREADD activation of PVN^{MC4R+} neurons suppress feeding but not glucose homeostasis

To evaluate the functional role of PVN^{MC4R+} neurons, hM3Dq-DREADD-mediated activation of PVN^{MC4R+} neurons was performed. Bilateral microinjection of Cre-dependent AAV-DIO-hM3Dq-mCherry into the PVN of MC4R-Cre+ mice resulted in activation of PVN^{MC4R+} neurons, as assessed by double fluorescent IHC for mCherry and c-Fos (Supplemental Figure 3A and B), an established marker of neuronal activation. After confirming the effective DREADD-mediated activation of PVN^{MC4R+} neurons, we first tested the effects of DREADD activation of PVN^{MC4R+} neurons on feeding and glucoregulation. As previously shown [24], DREADD activation of PVN^{MC4R+} neurons right before the onset of dark cycle significantly suppressed feeding (Supplemental Figure 3C), which was not observed when CNO was administered to control mice without hM3Dq-DREADD expression (Supplemental Figure 4A). Contrastively, neither baseline glucose nor glucose tolerance was affected by DREADD activation of PVN^{MC4R+} neurons (Supplemental Figure 3D–E). Importantly, these observations were supported in an independent experimental cohort of MC4R-Cre+ male mice that received either AAV2-DIO-hM3Dq-mCherry (DREADD group, $n = 8$) or AAV2-DIO-mCherry (control group, $n = 7$) into the PVN. Effective activation (c-Fos) of PVN^{MC4R+} neurons was only observed in the DREADD group, but not the control group, upon IP injection of CNO (2 mg/kg) (Figure 3A–C). Continuous monitoring of food intake with FED3 attached to home cage revealed that IP injection of CNO right before dark phase significantly suppress food intake in DREADD group compared to control group (Figure 3D). GTT with 15-min pretreatment of CNO in 5-hour fasted mice again revealed no effect of the DREADD activation of PVN^{MC4R+} neurons on systemic glucose homeostasis (Figure 3E).

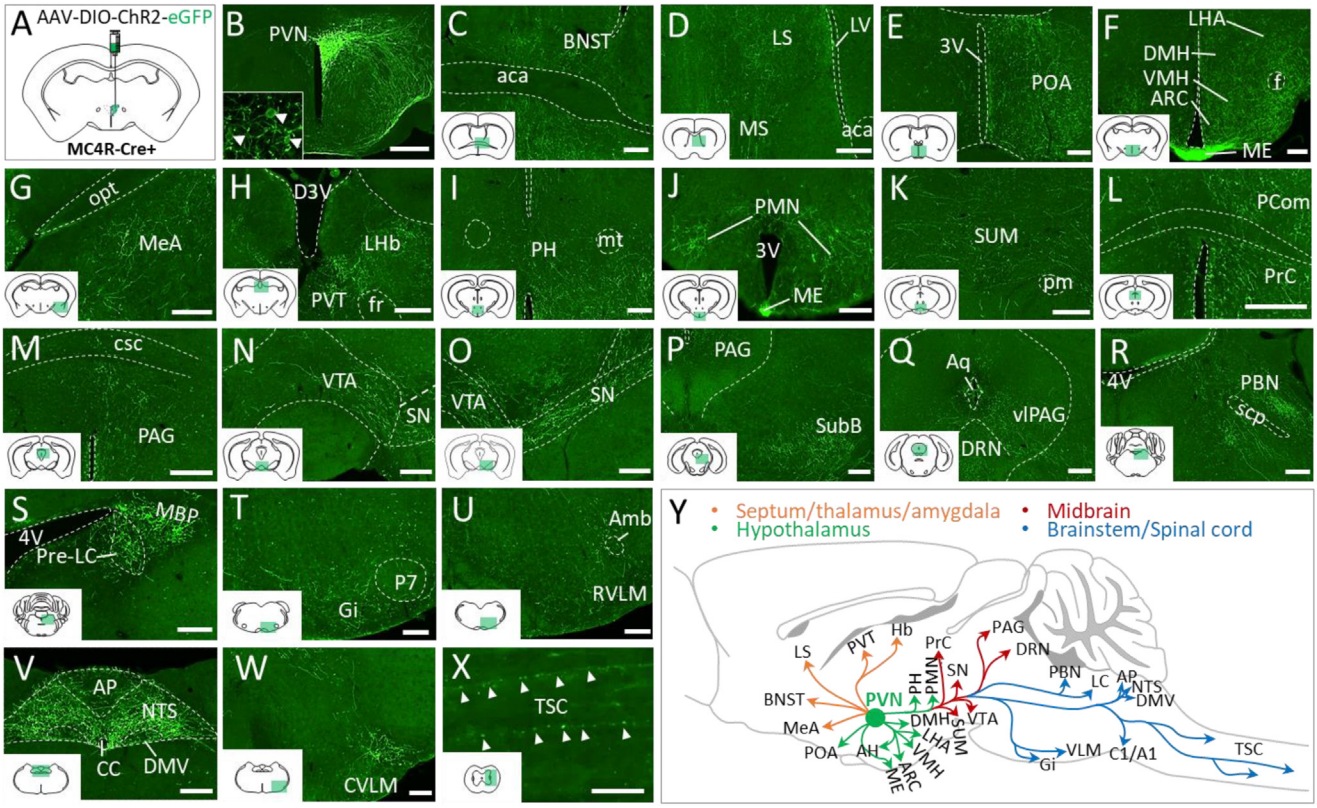

Figure 1: Whole-brain mapping of efferent projections of PVN^{MC4R+}neurons. (**A**) Schematic showing unilateral viral injection into the PVN of MC4R-Cre^{+} mouse for anterograde tract-tracing (n = 4). (**B**) Representative image showing unilateral GFP expression in the PVN^{MC4R+} neurons. Inset shows cell bodies of PVN^{MC4R+} neurons expressing GFP. (**C**–**W**) Representative images showing the projections of PVN^{MC4R+} neurons to different brain regions. (**Y**) Schematic depicting major PVN^{MC4R+} axonal projections throughout the brain. Abbreviations: bed nucleus of the stria terminalis (BNST), lateral (LS), medial septum (MS), preoptic area (POA), dorsomedial hypothalamic nucleus (DMH), ventromedial hypothalamic nucleus (VMH), lateral hypothalamic area (LHA), arcuate hypothalamic nucleus (ARC), median eminence (ME), medial amygdaloid nucleus (MeA), lateral habenular nucleus (LHb), paraventricular nucleus of the thalamus (PVT), posterior hypothalamic nucleus (PH), premammillary nucleus (PMN), Supramammillary nucleus (SUM), nucleus of the posterior commissure (Pcom), precommissural nucleus (Prc), periaqueductal grey (PAG), ventral tegmental area (VTA), substantia nigra (SN), subbrachial nucleus (SubB), dorsal raphe nucleus (DRN), ventrolateral PAG (vlPAG), parabrachial nucleus (PBN), pre-locus coeruleus (pre-LC), medial PBN (MBP), Gigantocellular reticular nucleus (Gi), Rostral ventrolateral medulla (RVLM), nucleus of solitary tract (NTS), dorsal motor nucleus of the vagus (DMV), area postrema (AP), Caudal ventrolateral medulla (CVLM), and thoracic spinal cord (TSC), lateral ventricle (LV), anterior commissure, anterior part (aca), 3rd ventricle (3V), fornix (f), optic tract (opt), dorsal 3rd ventricle (D3V), (fr), mammillothalamic tract (mt), principal mammillary tract (pm), posterior commissure (pc), commissure of the superior colliculus (csc), aqueduct (Aq), 4th ventricle (4V), superior cerebellar peduncle (scp), perifacial zone (P7), ambiguus nucleus (Amb), central canal (CC). Scale bar: 200 μm for B–W, 50 μm for X.

3.4. DREADD activation of PVN^{MC4R+} neurons affect thermoregulation

In contrast to the well-established role in feeding regulation, the role of PVN^{MC4R+} pathways in autonomic activity-driven thermoregulation remains unclear. Based on the observation of broad innervation of PVN^{MC4R+} neurons to many brain regions involved in sympathetic activation and thermoregulation (Figure 1Y), we next tested whether PVN^{MC4R+} circuits also affect autonomic thermoregulation. To this end, mice were placed on the treadmill for slow walking and body surface temperature was monitored by a high-resolution IR thermal imaging camera as the baseline. Mice then sequentially received IP injection of saline and CNO (2 mg/kg) with 1-hour interval and body surface temperature was taken 1-hour post-injection to evaluate the changes of body surface temperature. While IP saline did not result in notable changes in temperature as expected, there was an obvious increase in body surface temperature after 1-hour IP CNO (Figure 4A). Quantification revealed that DREADD activation of PVN^{MC4R+} neurons significantly increases the temperature in the neck area (brown fat), low back and tail (Figure 4B). The changes in temperature of the neck area and low back were not observed when CNO was given to control mice without hM3Dq-DREADD expression; however, there was a slight but significant increase in tail temperature after CNO treatment in control mice (Supplemental Figure 4B). Literature indicates that increased tail temperature is an indication of vasodilation which occur in rodents as a mean to promote heat dissipation and reduce body temperature [37]. Therefore, DREADD activation of PVN^{MC4R+} neurons may have caused an increase in core body temperature, leading to a counter-regulatory heat-dissipating response by promoting vasodilation. To directly test this possibility, we implanted a temperature transponder into the abdominal cavity of both DREADD and control mice and monitored the core body temperature upon IP injection of CNO. As we predicted, DREADD activation of PVN^{MC4R+} neurons caused a slight but significant increase in core body temperature compared to control mice (Figure 4C).

3.5. DREADD activation of PVN^{MC4R+} neurons increase BP and HR

Neurons in the PVN are critical in determining the sympathetic tone to the cardiovascular system and thereby affect BP and HR. We observed dense projections of PVN^{MC4R+} neurons to brain regions that are important for cardiovascular control, including PAG, NTS, RVLM, and

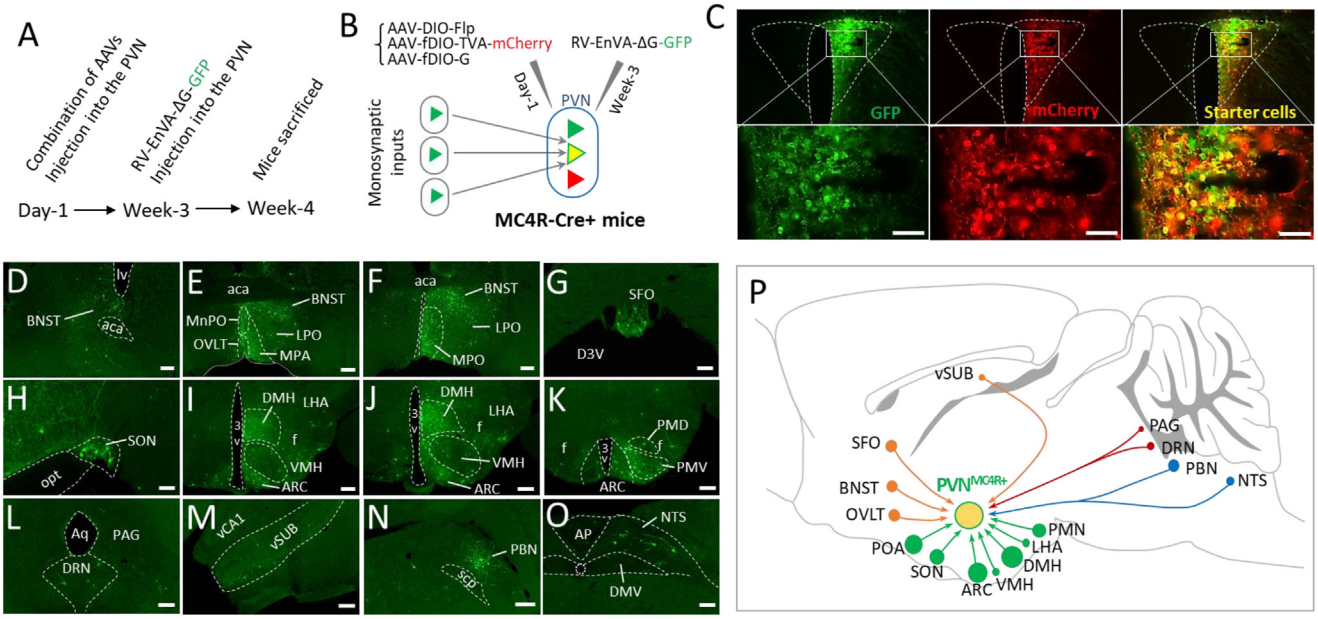

Figure 2: Monosynaptic inputs to PVN^{MC4R+}neurons. (**A**) Experimental timeline showing sequential viral injection (n = 4). (**B**) Schematic showing the viral strategy to map the neurons sending monosynaptic inputs to PVN^{MC4R+} neurons. (**C**) Representative images showing the successful targeting of PVN with different viral vectors. (**D**–**O**), Representative images showing GFP-positive cells observed throughout different brain regions. (**P**) Schematic depicting brain regions where neurons send monosynaptic inputs to PVN^{MC4R+} neurons. Note that the size of the filled circle in each brain region represents the relative optical density of observed GFP^{+} cells (smallest circle represents few scattered cells and the largest circle represents a dense group of cells). Abbreviations: median preoptic nucleus (MnPO), organum vasculosum of the lamina terminalis (OVLT), medial preoptic area (MPA), medial preoptic nucleus (MPO), lateral preoptic nucleus (LPO), subfornical organ (SFO), supraoptic nucleus (SON), dorsal premammillary nucleus (PMD), ventral premammillary nucleus (PMV), ventral hippocampal CA1 (vCA1), ventral subiculum (vSUB). Scale bar: 50 μm for C, 100 μm for G, H and O, 200 μm for D, E, F, I, J, K, L, M, and N.

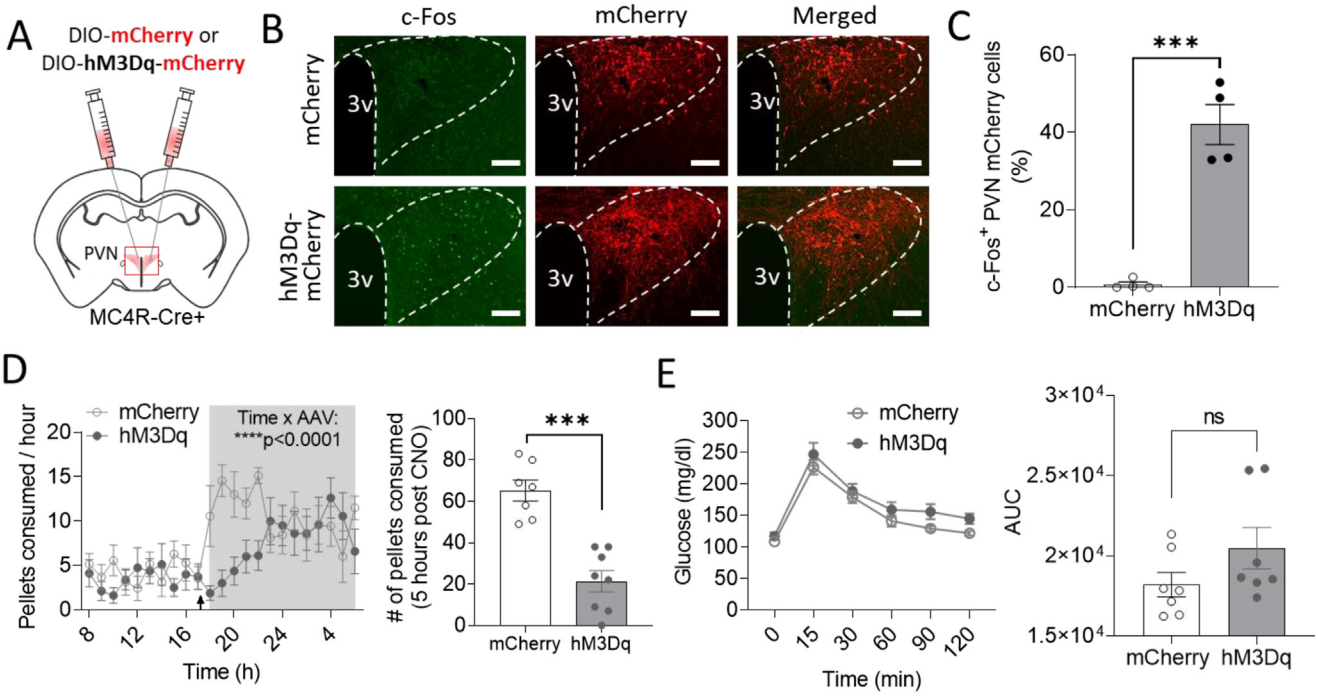

Figure 3: The effect of DREADD activation of PVN^{MC4R+}neurons on feeding and glucose homeostasis. (**A**) Schematic showing bilateral microinjection of Cre-dependent AAV driving expression of excitatory hM3Dq-DREADD receptor into the PVN of MC4R-Cre^{+} mouse. (**B**) Representative images showing mCherry and c-Fos immunoreactivity in the PVN of MC4R-Cre^{+} mice that received either AAV-DIO-mCherry or AAV-DIO-hM3Dq-mCherry (Scale bar: 100 μm). (**C**) Quantification of c-Fos^{+} PVN mCherry cells. (**D**) Decreased food pellets consumption (FED3) after IP injection of CNO at the beginning of dark cycle. (**E**) The effects of DREADD activation of PVN^{MC4R+} neurons on GTT (n = 7 for mCherry and n = 8 for hM3Dq). ***p < 0.001 by Student's t-test (C and pellets consumed 5 h post CNO in D) or by two-way ANOVA (time course pellets consumption in D). Data are presented as mean ± SEM.

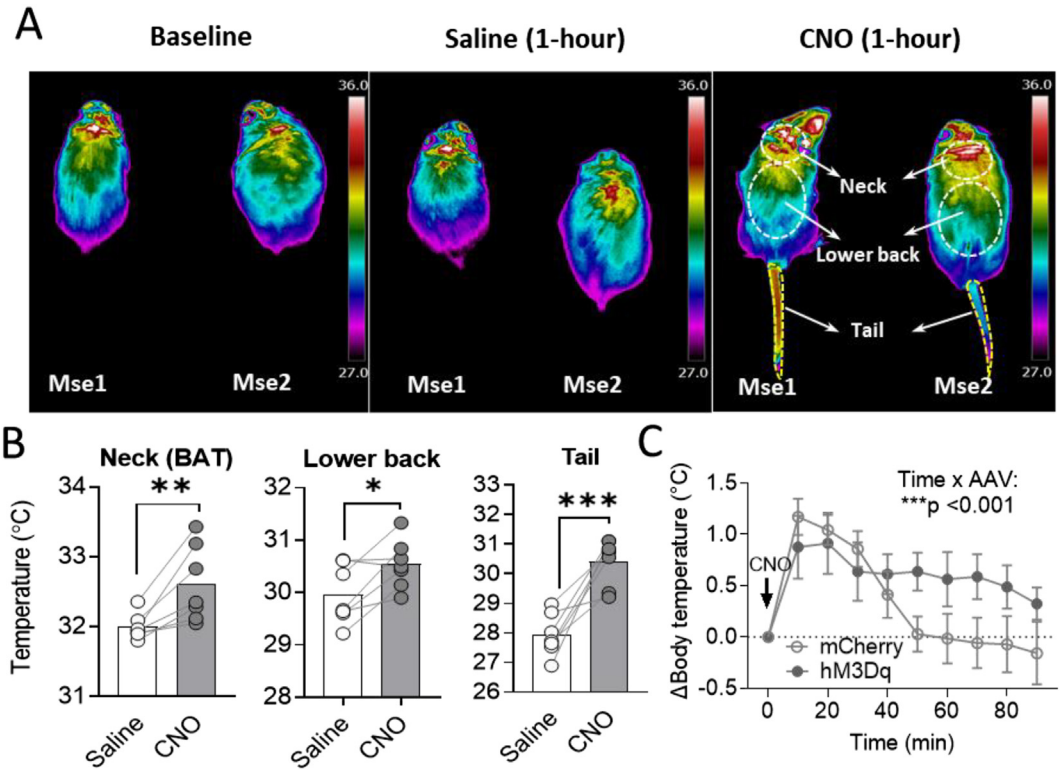

Figure 4: Thermoregulatory effect of DREADD activation of PVN^{MC4R+} neurons. (**A**) Representative IR thermographic images taken at baseline and after 60 min of saline or CNO treatment while allowing slow walking on a treadmill. Body surface areas of interest were drawn separately for the neck (BAT), lower back, and tail. (**B**) Quantified body surface temperature in mice received saline and CNO treatment (n = 7 mice). (**C**) Changes in core body temperature after CNO treatment in MC4R-Cre+ mice received AAV2-DIO-mCherry (control group, n = 7) or AAV2-DIO-hM3Dq-mCherry (DREADD group, n = 8) injection into the PVN. *P < 0.05, **P < 0.01**, ***P < 0.001 by paired Student's t-test (B) or by two-way ANOVA (C).

TSC (Figure 1). Therefore, we tested whether PVN^{MC4R+} neuron activation also alters BP and HR. To ascertain this, the mice were implanted with radio-telemeters for continuous monitoring of BP and HR. After two weeks of recovery from the surgery, mice were tested for their cardiovascular response to IP injection of either saline or CNO in both light and dark phases. Consistent with broad projections to various cardiovascular brain regions, DREADD activation of PVN^{MC4R+} neurons by a single dose of CNO (2 mg/kg) resulted in a sharp increase in MAP and HR in DREADD mice compared to control mice (Figure 5A–D). These cardiovascular responses elicited by DREADD activation of PVN^{MC4R+} neurons were apparent in the light cycle but not the dark cycle. Further analysis revealed that DREADD activation of PVN^{MC4R+} neurons increased both systolic arterial pressure (SAP) and diastolic arterial pressure (DAP) in the light cycle (Figure 5E–H). Importantly, CNO administration in non-DREADD control mice did not affect BP and HR (Supplemental Figure 4C–F).

3.6. Behavioral alterations by DREADD activation of PVN^{MC4R+} neurons

Because of the broad innervation of PVN^{MC4R+} neurons to diverse brain regions that are important for behavioral regulation (BNST, LHA, VTA, PAG, etc), we also tested whether activation of PVN^{MC4R+} neurons elicits other behavioral responses. To this end, we subjected mice to PhenoTyper cages which allow continued monitoring of different mouse behaviors in an automated manner. After overnight acclimation in the PhenoTyper cages, mice were given IP injection of either saline or CNO right before dark cycle (17:30–18:00) and then again next morning (8:00–9:00) to determine behavioral alterations in both dark and light cycles. The floor was further marked for 4 sub-arenas representing wheel running, food, water, and shelter zones, respectively (Figure 6A,B), which enable the calculation of time spent in each zone. We found that DREADD activation of PVN^{MC4R+} neurons led to an initial transient (1-hour post-injection) increase followed by significant suppression of ambulatory activity and body mobility (Figure 6C,D). The mice also spent more time in the shelter zone but less time in the food zone upon DREADD activation of PVN^{MC4R+} neurons (Figure 6E,F). No alteration in water drinking behavior was observed (Figure 6G). Consistent with reduced ambulatory activity, voluntary wheel running activity was also significantly reduced upon DREADD activation of PVN^{MC4R+} neurons (Figure 6H).

4. DISCUSSION

The PVN is a key node in the brain orchestrating a wide range of physiological and behavioral responses, including but not limited to fear, fight-or-flight response, feeding, metabolic homeostasis, and autonomic regulation of cardiovascular function. PVN^{MC4R+} neurons represent a small subset of PVN neurons; they are largely distinct from many well-known PVN neurons expressing different neuropeptides [20,38]. Substantial evidence supports a role for PVN^{MC4R+} pathways in feeding regulation mainly via PVN^{MC4R+} → PBN circuit [23,24,39]. In the current study, we provide further evidence to show a rather complex role of PVN^{MC4R+} neurons beyond feeding.

We observed a significant increase in body surface temperature around the neck and lower back upon DREADD activation of PVN^{MC4R+} neurons, indicating a likely elevation of sympathetic drive to

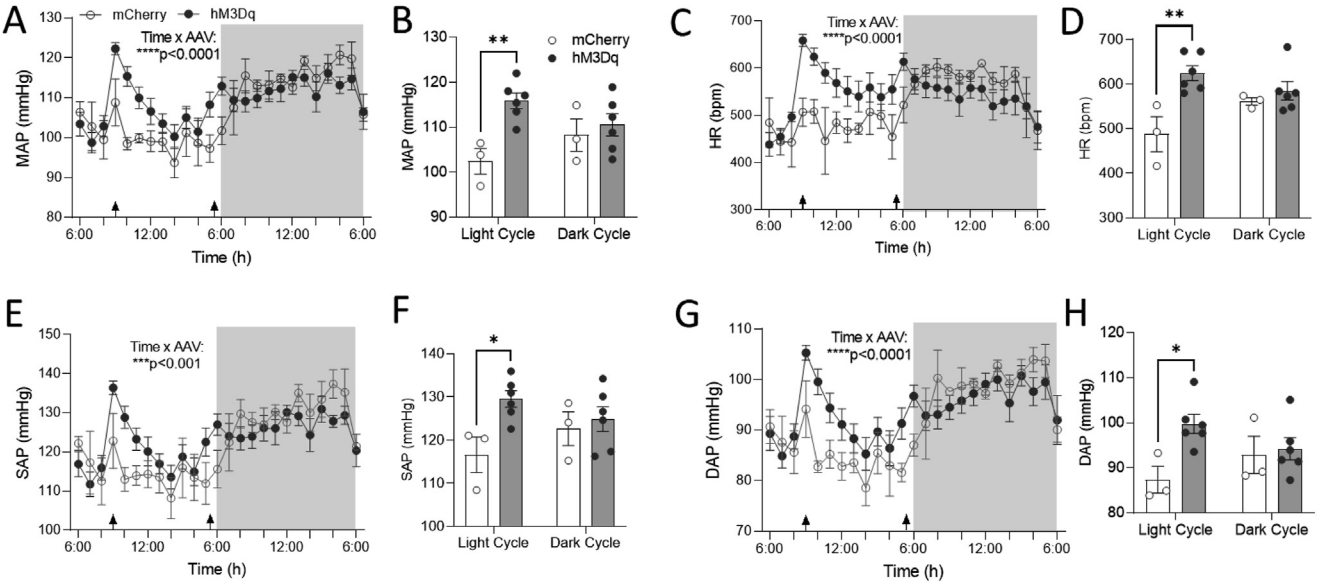

Figure 5: The effects of chemogenetic activation of PVN^{MC4R+} neurons on cardiovascular function. MC4R-Cre^{+} mice expressing either mCherry (n = 3) or hM3Dq-mCherry (n = 6) in the PVN were implanted with DSI radiotelemetry for continuous monitoring of BP and HR. Mice were given IP injection of CNO in the morning and then again in the evening right before dark cycle (arrows on the X-axis indicate the time of each treatment). (**A, C, E, G**) MAP (**A**), HR (**C**), SAP (**E**), and DAP (**G**) were analyzed hourly and compared between the groups. (**B, D, F, H**) The average of 3-hour post-treatment for MAP (**B**), HR (**D**), SAP (**F**), DAP (**H**) was also analyzed separately for light and dark cycles and compared between the groups. *P $\leq$ 0.05, **P $<$ 0.01, ***P $<$ 0.001 by two-way ANOVA. Data are presented as mean $\pm$ SEM.

the BAT. This observation supports a previous findings that PVN^{MC4R+} neurons polysynaptically innervate the BAT [40,41], intra-PVN injection of MC4R agonist MTII increase BAT temperature [40], and selective restoration of MC4Rs in Sim-1^{+} neurons that predominantly localized to the PVN rescues blunted MTII-induced increase in energy expenditure in MC4R-null mice [42]. PVN^{MC4R+} neuron activation also increased the core body temperature, which might have caused a significantly increased tail temperature—an indication of vasodilation that promotes heat dissipation and reduces body temperature in rodents [37]. An increase in tail temperature and hence vasodilation suggests that DREADD activation of PVN^{MC4R+} neurons does not cause indiscriminate sympathoexcitation as is normally seen in an acute stress response, which should have caused vasoconstriction rather than vasodilation. Thus, PVN^{MC4R+} neurons may selectively influence sympathetic outflows to certain effector organs among others. Another possibility for increased body surface temperature could be due to an evoked neuroendocrine response, such as the activation of the hypothalamic-pituitary-thyroid (HPT) axis, which promotes metabolism and heat production. The densest innervation of PVN^{MC4R+} neurons was observed in the ME (Figure 1F and Supplemental Table 1). However, since previous studies have shown that there is minimal overlap of PVN^{MC4R+} neurons with thyrotropin-releasing hormone (TRH) [20,38], it remains to be seen whether PVN^{MC4R+} neurons can activate the HPT axis. Functional roles of the PVN^{MC4R+} $\rightarrow$ ME/pituitary pathway, therefore, warrants further investigation.

In addition to metabolic homeostasis, it has been well established that brain MC4R signaling pathways affect sympathetic control of cardiovascular function, which has been an obstacle for developing a safe anti-obesity medication by targeting MC4Rs [6]. MC4Rs are broadly expressed in different brain regions involving in autonomic control of cardiovascular function [20], and our results now support the idea that PVN could be one of the important brain regions where MC4R signaling affects cardiovascular physiology. We observed a sharp increase in MAP and HR upon DREADD activation of PVN^{MC4R+} neurons, especially when neurons are activated in the light cycle, but not the dark cycle. The peak responses of BP and HR were even higher when activated in the light cycle compared to the dark cycle (Figure 5). The underlying mechanism of this light phase-specific rise in BP and HR by PVN^{MC4R+} neuron activation remains unclear but may involve circadian-specific responses of effector organs (vasculature and heart) to a sudden increase in sympathetic outflow. Our findings are consistent with previous pharmacological observations showing that intra-PVN injection of MTII increases MAP in anesthetized lean Zucker rats [25] and that MTII-mediated increase in BP is lost in mice lacking Gαs in PVN neurons [26], arguing a plausible role of PVN^{MC4R} signaling in sympathetic control of cardiovascular function.

Behavioral monitoring in PhenoTyper cages unexpectedly revealed that DREADD activation of PVN^{MC4R+} neurons acutely increases ambulatory movements followed by an obvious behavioral suppression, including reduced locomotor activity, feeding and voluntary wheel running. These behavioral suppressions indicate that increase in BP and HR is unlikely secondary to the behavioral alterations, implying there could be segregated PVN^{MC4R+} pathways that differentially mediate behavioral and autonomic responses. Indeed, our anterograde tract-tracing revealed that PVN^{MC4R+} neurons broadly innervate many different brain regions known to mediate different behavioral and physiological responses. Because of the well-known cardiovascular side effects of pharmacological activation of MC4R signaling, it is of significant interest for future studies to test whether there are anatomically distinct subsets of PVN^{MC4R+} neurons that differentially regulate feeding behavior and sympathetic control of cardiovascular function. For instance, several studies have shown that the PVN^{MC4R+} $\rightarrow$ PBN and PVN^{MC4R+} $\rightarrow$ pre-LC pathways can reduce feeding [23,24,39]; however, whether these pathways also affect cardiovascular function is unknown. Our anterograde tracing clearly shows that in addition to the PBN, PVN^{MC4R+} neurons also heavily innervate brain regions involved in sympathetic control of cardiovascular function, including NTS, VML,

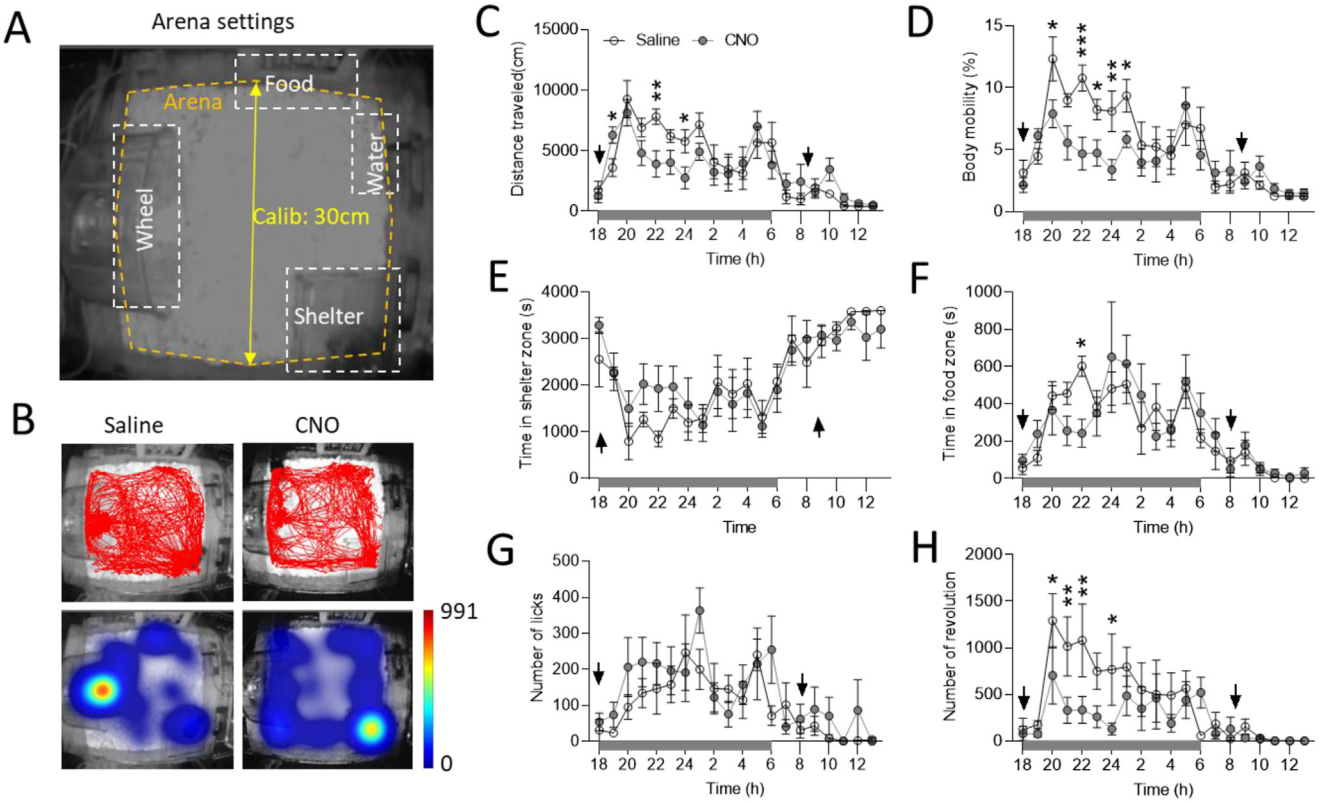

Figure 6: Automated behavioral analysis of mice with DREADD activation of PVN^{MC4R+} neurons in PhenoTyper boxes. (**A**) Representative schematic showing arena setting in PhenoTyper cage for behavioral characterization. (**B**) Representative activity trace (upper panel) and heat map (lower panel) showing total distance traveled and the time spent in each zone after either saline or CNO treatment. (**C**–**H**) Hourly quantitative analysis showing total distance traveled (**C**), body mobility (**D**), time spent in shelter zone (**E**), time spent in food zone (**F**), number of water licks (**G**), and the total number of wheel running (**H**) in response to saline and CNO treatment (arrows on the X-axis indicate the time of injection in the morning and the evening; n = 7/group). *P < 0.05, **P < 0.01, ***P < 0.001 by multiple t-test. Data are presented as mean ± SEM.

PAG, and TSC. However, the functional roles of these projections in the sympathetic control of cardiovascular function have not yet been explored. Another important question that arose from the present study is whether PVN^{MC4R+} neurons send collateral projections to different brain regions to simultaneously affect both feeding and autonomic control of cardiovascular function and thermoregulation. More refined functional circuit mapping studies are needed to answer these important yet unresolved questions in the future.

There are some limitations of the current study. Although viral-mediated axonal tracing is widely used nowadays to delineate cell-type-specific brain circuits, whether most ChR2-eYFP fibers we observed across the brain regions make functional synaptic connections remains unclear. It is possible that some ChR2-eYFP fibers in certain brain regions could be just passing-through axons. Comprehensive ChR2-assisted circuit mapping with electrophysiological recording in those projected brain regions is required to prove the likelihood of true synaptic connections in future studies. Additionally, it is challenging to robustly cover the entire rostral-to-caudal structure of PVN without contaminating adjacent brain regions by stereotaxic injection; therefore, neuroanatomical mapping of both efferent and afferent circuits we presented here could have underestimated the actual input–output organization of PVN^{MC4R+} neurons. Another potential concern is the use of CNO as an option for neuronal activation. Studies have shown that when used in high dose (>5 mg/kg), CNO can be reverse-metabolized into clozapine [43,44], an antipsychotic medication that could impact some behaviors and physiological measurements. While we did not observe significant effects of CNO on feeding, BAT temperature, and cardiovascular parameters in control mice, the tail temperature was found slightly but significantly increased by CNO treatment in control mice (although the effect was much smaller than that of DREADD activation of PVN^{MC4R+} neurons). Since clozapine has been shown to have a vasodilatory effect [45,46], we speculate that this small increase of tail temperature could be due to vasodilation caused by clozapine that converted from CNO. It is therefore worthwhile to test in the future whether optogenetic activation of PVN^{MC4R+} neurons can replicate some of the functional observations made in the present study.

5. CONCLUSION

In summary, we mapped the neuroanatomical connections of PVN^{MC4R+} neurons and present further evidence to show that PVN^{MC4R+} circuits mediate complex behavioral and physiological regulations beyond feeding. PVN^{MC4R+} signaling pathways have been the focus of appetite suppression for potential anti-obesity therapeutics. Understanding the neural basis of PVN^{MC4R+} signaling pathways for these additional behavioral and physiological regulations may therefore help to refine the strategy for targeting PVN^{MC4R+} to treat obesity and associated complications, such as obesity-associated hypertension.

AUTHOR CONTRIBUTIONS

US and HC contributed to conceptualization, study design, methodology, and manuscript writing. US, JJ, KS, BAT, JED, SRR, YD, GD, BX, ZZ, JCG, and LVZ conducted and/or provided critical technical assistance for the experiments. US and HC contributed to the data analysis.

ACKNOWLEDGMENTS

We would like to thank Dr. Bradford Lowell (Beth Israel Deaconess Medical Center, Boston, MA) for the use of the *MC4R*-Cre mouse line. This work was supported by grants from the National Institutes of Health (HL153274, HL127673 and HL084207 to HC), the University of Iowa Fraternal Order of Eagles Diabetes Center Pilot Grant (to HC), and the American Heart Association (19POST34450083 to US, 19POST34380239 to GD).

CONFLICT OF INTEREST

None declared.

APPENDIX A. SUPPLEMENTARY DATA

Supplementary data to this article can be found online at https://doi.org/10.1016/j.molmet.2021.101401.

REFERENCES

[1] Krauss, R.M., Winston, M., Fletcher, B.J., Grundy, S.M., 1998. Obesity : impact on cardiovascular disease. Circulation 98(14):1472—1476.

[2] Tentolouris, N., Liatis, S., Katsilambros, N., 2006. Sympathetic system activity in obesity and metabolic syndrome. Annals of the New York Academy of Sciences 1083:129—152.

[3] Grassi, G., Biffi, A., Seravalle, G., Trevano, F.Q., Dell'Oro, R., Corrao, G., et al., 2019. Sympathetic neural overdrive in the obese and overweight state. Hypertension 74(2):349—358.

[4] do Carmo, J.M., da Silva, A.A., Wang, Z., Fang, T., Aberdein, N., Perez de Lara, C.E., et al., 2017. Role of the brain melanocortins in blood pressure regulation. Biochimica et Biophysica Acta - Molecular Basis of Disease 1863(10 Pt A):2508—2514.

[5] da Silva, A.A., do Carmo, J.M., Hall, J.E., 2013. Role of leptin and central nervous system melanocortins in obesity hypertension. Current Opinion in Nephrology and Hypertension 22(2):135—140.

[6] da Silva, A.A., do Carmo, J.M., Wang, Z., Hall, J.E., 2019. Melanocortin-4 receptors and sympathetic nervous system Activation in hypertension. Current Hypertension Reports 21(6):46.

[7] da Silva, A.A., do Carmo, J.M., Wang, Z., Hall, J.E., 2014. The brain melanocortin system, sympathetic control, and obesity hypertension. Physiology 29(3):196—202.

[8] Huszar, D., Lynch, C.A., Fairchild-Huntress, V., Dunmore, J.H., Fang, Q., Berkemeier, L.R., et al., 1997. Targeted disruption of the melanocortin-4 receptor results in obesity in mice. Cell 88(1):131—141.

[9] Yeo, G.S., Farooqi, I.S., Aminian, S., Halsall, D.J., Stanhope, R.G., O'Rahilly, S., 1998. A frameshift mutation in MC4R associated with dominantly inherited human obesity. Nature Genetics 20(2):111—112.

[10] Kuo, J.J., Silva, A.A., Hall, J.E., 2003. Hypothalamic melanocortin receptors and chronic regulation of arterial pressure and renal function. Hypertension 41(3 Pt 2):768—774.

[11] Rahmouni, K., Haynes, W.G., Morgan, D.A., Mark, A.L., 2003. Role of melanocortin-4 receptors in mediating renal sympathoactivation to leptin and insulin. Journal of Neuroscience 23(14):5998—6004.

[12] Tallam, L.S., da Silva, A.A., Hall, J.E., 2006. Melanocortin-4 receptor mediates chronic cardiovascular and metabolic actions of leptin. Hypertension 48(1):58—64.

[13] Greenfield, J.R., Miller, J.W., Keogh, J.M., Henning, E., Satterwhite, J.H., Cameron, G.S., et al., 2009. Modulation of blood pressure by central melanocortinergic pathways. New England Journal of Medicine 360(1):44—52.

[14] Greenfield, J.R., 2011. Melanocortin signalling and the regulation of blood pressure in human obesity. Journal of Neuroendocrinology 23(2):186—193.

[15] Tallam, L.S., Stec, D.E., Willis, M.A., da Silva, A.A., Hall, J.E., 2005. Melanocortin-4 receptor-deficient mice are not hypertensive or salt-sensitive despite obesity, hyperinsulinemia, and hyperleptinemia. Hypertension 46(2):326—332.

[16] Sayk, F., Heutling, D., Dodt, C., Iwen, K.A., Wellhoner, J.P., Scherag, S., et al., 2010. Sympathetic function in human carriers of melanocortin-4 receptor gene mutations. The Journal of Cinical Endocrinology and Metabolism 95(4):1998—2002.

[17] do Carmo, J.M., da Silva, A.A., Hall, J.E., 2015. Role of hindbrain melanocortin-4 receptor activity in controlling cardiovascular and metabolic functions in spontaneously hypertensive rats. Journal of Hypertension 33(6):1201—1206.

[18] Haynes, W.G., Morgan, D.A., Djalali, A., Sivitz, W.I., Mark, A.L., 1999. Interactions between the melanocortin system and leptin in control of sympathetic nerve traffic. Hypertension 33(1 Pt 2):542—547.

[19] Geerling, J.C., Shin, J.W., Chimenti, P.C., Loewy, A.D., 2010. Paraventricular hypothalamic nucleus: axonal projections to the brainstem. Journal of Comparative Neurology 518(9):1460—1499.

[20] Kishi, T., Aschkenasi, C.J., Lee, C.E., Mountjoy, K.G., Saper, C.B., Elmquist, J.K., 2003. Expression of melanocortin 4 receptor mRNA in the central nervous system of the rat. Journal of Comparative Neurology 457(3):213—235.

[21] Liu, H., Kishi, T., Roseberry, A.G., Cai, X., Lee, C.E., Montez, J.M., et al., 2003. Transgenic mice expressing green fluorescent protein under the control of the melanocortin-4 receptor promoter. Journal of Neuroscience 23(18):7143—7154.

[22] Balthasar, N., Dalgaard, L.T., Lee, C.E., Yu, J., Funahashi, H., Williams, T., et al., 2005. Divergence of melanocortin pathways in the control of food intake and energy expenditure. Cell 123(3):493—505.

[23] Shah, B.P., Vong, L., Olson, D.P., Koda, S., Krashes, M.J., Ye, C., et al., 2014. MC4R-expressing glutamatergic neurons in the paraventricular hypothalamus regulate feeding and are synaptically connected to the parabrachial nucleus. Proceedings of the National Academy of Sciences of the United States of America 111(36):13193—13198.

[24] Garfield, A.S., Li, C., Madara, J.C., Shah, B.P., Webber, E., Steger, J.S., et al., 2015. A neural basis for melanocortin-4 receptor-regulated appetite. Nature Neuroscience 18(6):863—871.

[25] Li, P., Cui, B.P., Zhang, L.L., Sun, H.J., Liu, T.Y., Zhu, G.Q., 2013. Melanocortin 3/4 receptors in paraventricular nucleus modulate sympathetic outflow and blood pressure. Experimental Physiology 98(2):435—443.

[26] Li, Y.Q., Shrestha, Y., Pandey, M., Chen, M., Kablan, A., Gavrilova, O., et al., 2016. G(q/11)alpha and G(s)alpha mediate distinct physiological responses to central melanocortins. Journal of Clinical Investigation 126(1):40—49.

[27] Ye, Z.Y., Li, D.P., 2011. Activation of the melanocortin-4 receptor causes enhanced excitation in presympathetic paraventricular neurons in obese Zucker rats. Regulatory Peptides 166(1—3):112—120.

[28] Cui, H., Sohn, J.W., Gautron, L., Funahashi, H., Williams, K.W., Elmquist, J.K., et al., 2012. Neuroanatomy of melanocortin-4 receptor pathway in the lateral hypothalamic area. Journal of Comparative Neurology 520(18):4168—4183.

[29] Cui, H., Lu, Y., Khan, M.Z., Anderson, R.M., McDaniel, L., Wilson, H.E., et al., 2015. Behavioral disturbances in estrogen-related receptor alpha-null mice. Cell Reports 11(3):344—350.

[30] Matikainen-Ankney, B.A., Earnest, T., Ali, M., Casey, E., Sutton, A.K., Legaria, A., et al., 2020. Feeding Experimentation Device version 3 (FED3): an open-source home-cage compatible device for measuring food intake and operant behavior. bioRxiv.

[31] Zhu, Z., Sierra, A., Burnett, C.M., Chen, B., Subbotina, E., Koganti, S.R., et al., 2014. Sarcolemmal ATP-sensitive potassium channels modulate skeletal muscle function under low-intensity workloads. The Journal of General Physiology 143(1):119—134.

[32] Zingman, L.V., Hodgson, D.M., Bast, P.H., Kane, G.C., Perez-Terzic, C., Gumina, R.J., et al., 2002. Kir6.2 is required for adaptation to stress. Proceedings of the National Academy of Sciences of the United States of America 99(20):13278—13283.

[33] Pham, J., Cabrera, S.M., Sanchis-Segura, C., Wood, M.A., 2009. Automated scoring of fear-related behavior using EthoVision software. Journal of Neuroscience Methods 178(2):323—326.

[34] Jiang, J., Morgan, D.A., Cui, H., Rahmouni, K., 2020. Activation of hypothalamic AgRP and POMC neurons evokes disparate sympathetic and cardiovascular responses. American Journal of Physiology - Heart and Circulatory Physiology 319(5):H1069—H1077.

[36] Krashes, M.J., Shah, B.P., Madara, J.C., Olson, D.P., Strochlic, D.E., Garfield, A.S., et al., 2014. An excitatory paraventricular nucleus to AgRP neuron circuit that drives hunger. Nature 507(7491):238—242.

[37] Tsuchiya, K., 2001. The rat tail as a Model organ for peripheral vasodilation. p. 192—9.

[38] Li, C., Navarrete, J., Liang-Guallpa, J., Lu, C., Funderburk, S.C., Chang, R.B., et al., 2019. Defined paraventricular hypothalamic populations exhibit differential responses to food contingent on caloric state. Cell Metabolism 29(3):681—694 e685.

[39] Li, M.M., Madara, J.C., Steger, J.S., Krashes, M.J., Balthasar, N., Campbell, J.N., et al., 2019. The paraventricular hypothalamus regulates satiety and prevents obesity via two genetically distinct circuits. Neuron 102(3):653—667 e656.

[40] Song, C.K., Vaughan, C.H., Keen-Rhinehart, E., Harris, R.B., Richard, D., Bartness, T.J., 2008. Melanocortin-4 receptor mRNA expressed in sympathetic outflow neurons to brown adipose tissue: neuroanatomical and functional evidence. American Journal of Physiology - Regulatory, Integrative and Comparative Physiology 295(2):R417—R428.

[41] Voss-Andreae, A., Murphy, J.G., Ellacott, K.L., Stuart, R.C., Nillni, E.A., Cone, R.D., et al., 2007. Role of the central melanocortin circuitry in adaptive thermogenesis of brown adipose tissue. Endocrinology 148(4):1550—1560.

[42] Xu, Y., Wu, Z., Sun, H., Zhu, Y., Kim, E.R., Lowell, B.B., et al., 2013. Glutamate mediates the function of melanocortin receptor 4 on Sim1 neurons in body weight regulation. Cell Metabolism 18(6):860—870.

[43] Manvich, D.F., Webster, K.A., Foster, S.L., Farrell, M.S., Ritchie, J.C., Porter, J.H., et al., 2018. The DREADD agonist clozapine N-oxide (CNO) is reverse-metabolized to clozapine and produces clozapine-like interoceptive stimulus effects in rats and mice. Scientific Reports 8(1):3840.

[44] Gomez, J.L., Bonaventura, J., Lesniak, W., Mathews, W.B., Sysa-Shah, P., Rodriguez, L.A., et al., 2017. Chemogenetics revealed: DREADD occupancy and activation via converted clozapine. Science 357(6350):503—507.

[45] Mateus, L.S., Albuquerque, A.A.S., Celotto, A.C., Evora, P.R.B., 2019. In vitro evidence that endothelium-dependent vasodilatation induced by clozapine is mediated by an ATP-sensitive potassium channel. Pharmacological Reports 71(3):522—527.

[46] Boussery, K., Lambrecht, S., Delaey, C., Van de Voorde, J., 2005. Clozapine directly relaxes bovine retinal arteries. Current Eye Research 30(2):139—146.

